A Study on Residual Fatigue Bending Strength and Damage Behavior of CFRP Composites Subjected to Impact Loadings

Kwang-Hee Im*, Jeong-Ho Kim* and In-Young Yang**

(Received January 30, 1997)

This paper evaluates the static and fatigue bending strengths of CFRP (carbon-fiber reinforced plastic) laminates having impact damages, e. g., foreign object damages (FOD). Composite laminates used in this experiment are CF/EPOXY and CF/PEEK orthotropy laminated plates with two-interfaces $[0°_4/90°_4]_s$. A steel ball launched by an air gun collides against the CFRP laminates to generate impact damages. The damage growth during a bending fatigue test is observed by a scanning acoustic microscope (SAM). When the impacted side is compressed, the residual fatigue bending strength of CF/PEEK specimen P is greater than that of CF/EPOXY specimen B. On the other hand, when the impacted side is in tension, the residual fatigue bending strength of CF/PEEK specimen P is smaller than that of CF/EPOXY specimen B. In the case of impacted-side compression, the fracture is propagated from the transverse crack generated near the impact point. In the case of impacted-side tension, however, the fracture develops toward the impact point from the edge of interface-B delamination

Key Words: Foreign Object Damages, Impact Damage, CFRP, Delamination Area, Impact Energy, Residual Bending Fatigue Strength

1. Introduction

Currently the importance of carbon-fiber reinforced plastics (CFRP) in both space and civil aircraft, which require superior stiffness and strength, have been generally recognized, and CFRPs are widely used due to their lightweight ratios compared to conventional metallic materials.

Unfortunately, CFRP laminates are too brittle for dynamic loadings, particularly impact loadings (Tanaka and Kurokawa, 1989), which can significantly reduce their properties. Therefore impact problems for a composites are becoming increasingly important. A dropped wrench, bird strike (Ma et al., 1991), or runway debris can generate localized delaminated areas of foreign object damage (FOD) (Takeda, 1985) by an impact which is frequently difficult to detect with the naked eye. Innocuous though this damage may seem in the stacking plates, it can result in premature catastrophic failure due to decreasing strength caused by impact loading.

Recently fatigue tests have been widely performed using FRP laminates and notched laminates in the case of FRP members subjected to cycle loadings. Rotem (Rotem et al., 1990), Bakis (Bakis et al., 1985) and Smith (Smith and Grove, 1987 and Yang et al., 1996) have studied the decreasing relationships of fatigue strength using of composites under cycle loadings. They only present a residual strength evaluation of the composites, but do not show a failure mechanism of residual fatigue strength decreased by using impact-induced laminates. Therefore, after a steel ball is impacted on the CFRP laminates, the static and fatigue bending strength is estimated according to the matrix, and the failure mechanisms are

* Graduate Student, Department of Mechanical Engineering, Chosun University 375 Sosok-dong, Dong-gu, Kwangju, 501-759, Korea

** Factory Automation Research Center for Parts of Vehicles Department of Mechanical Design Engineering, Chosun University 375 Sosok-dong, Dong-gu, Kwangju, 501-759, Korea

confirmed with the bases of damage development, which is observed by the SAM.

This paper attempts to evaluate the residual fatigue bending strength of laminates through the three-point bending fatigue test, and to confirm the failure mechanisms based on damage development.

Table 1 Characteristics of CF/EPOXY and CF/PEEK specimens.

Types / Characteristics	Carbon fiber	EPOXY resin	Prepreg
Maker	TORAY, Japan	TORAY, Japan	
Model	T300-3000	#2500	P. 3051-15
Density	1.75×10^3 [kg/m^3]	1.24×10^3 [kg/m^3]	
Tension strength	3.53[GPa]	0.078[GPa]	
Elastic modulus	230[GPa]	3.96[GPa]	
Elongation	1.5[%]	2.0[%]	
Resin content			37[% Wt]

Table 1 Continued.

Types / Characteristics	Carbon fiber	PEEK resin	Prepreg	
			0°	90°
Maker	TORAY, Japan	HWA S. Fiber, Japan		
Model	T300-3000	APC-2/AS4		
Density	1.75×10^3 [kg/m^3]	1.6×10^3 [kg/m^3]		
Tension strength	3.53[GPa]		2.13 [GPa]	0.008 [GPa]
Elastic modulus	230[GPa]		134 [GPa]	8.9 [GPa]
Elongation	1.5[%]		1.25	1.0
Resin content		32[%]		
Compression strength			1.1 [GPa]	
Bending strength			1.88 [GPa]	0.137 [GPa]

2. Experimental Method

2.1 Specimen configurations

The laminates of the specimens were manufactured from one-directional prepreg sheets of T300-3000 carbon fibers (#2500 EPOXY resin) and APC-2/AS4 carbon fibers/PEEK (CF/PEEK) in Japan Toray P3051-15, cured to the manufacturer's specifications as shown in Table 1. Two types of specimens were used in this experimentation. The specimen types are as follows: CF/EPOXY laminates are specimen B and CF/PEEK laminates are specimen P. Their lay up, stacked with 16 plies, indicates that specimens B, P are all $[0°_4/90°_4]_S$. Test specimens were prepared with dimensions 40 mm × 180 mm × 3.75 mm (width × length × thickness).

The fiber-direction of the specimen surface is manufactured to correspond to a direction of 0o; thus, the fiber-direction is the same as the length direction. By regulating the width of unimpacted specimens larger than that of specimens generated by an impact load, it is possible that none of the experimental results are influenced by edge effects. By properly manipulating the hardening temperature point with the use of a heater at the vacuum bag of the autoclave, the CFRP laminates can be cured.

2.2 Impact experimentation

The test fixture consisted of two steel plates (10 mm in thickness) and two rubber plates (10 mm in thickness), which were cut with a circular hole (150 mm diameter) at the center of the plates. The specimen was supported in the space between the rubber plates with steel plates on each side. A steel ball 5 mm in diameter (0.5g) was impacted on the specimen by using compressed air as shown in Fig. 1.

The velocity of the steel ball was measured just before impact by determining the time taken for it to pass two fine laser beams located a known distance (10 mm) apart. The impact velocity was obtained by varying air pressures on a compressor. The impact energy was 1.71J (with a velocity of 82.64 m/s) and 2.50J (with a velocity of 100

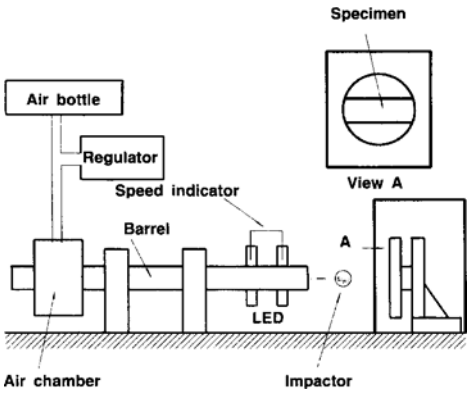

Fig. 1 Schematic of experimental setup.

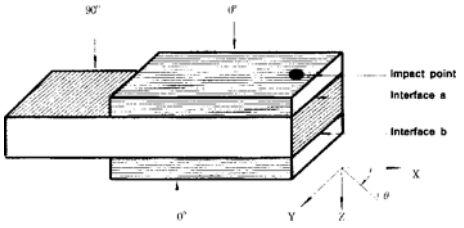

Fig. 2 Interfaces configuration for CFRP specimens B, P.

m/s). The impact energy (J) shows the kinetic energy of the impactor prior to impact.

2.3 Damage detection techniques

After impact, the delamination of specimen interfaces was assessed using an ultrasonic microscope (Olympus UH100 with the range of 30MHz). After performing the fatigue test, the damage growth is observed by separating a specimen from the fixture, and the test is performed again. After labeling each interface **a, b, c,** and **d** from the impact point as shown in Fig. 2, interface a on the impacted side is observed in the case of specimens B, P. and interface **b** on the opposite impacted side is observed.

The measurement methods for the delamination areas are as follows: each interface is classified according to colors, and the distributed range of each color is measured using an ultrasonic microscope. The ultrasonics of frequency such as a high -frequency voltage are sent to piezo transducers on the acoustic lens, and the ultrasonics can be convergent due to the spherical section of acoustic

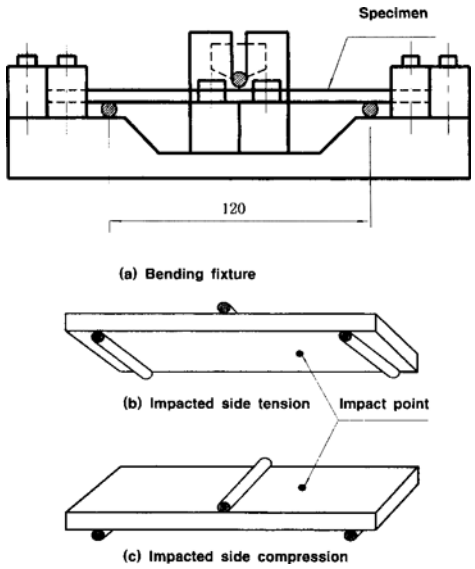

Fig. 3 Specimen supporting fixture of 3-point test.

lens, In order to magnify the medium from the lens, water greater than the density of air is used as the medium.

2.4 Fatigue three-point bending test

To examine residual bending fatigue strength of the specimen subjected to impact damages and to observe the damage in the specimen, a fatigue three-point bending test was carried out. Fig. 3 (a) shows the fixture attached to the universal testing machine (Instron 8501) for the experiments of impacted-side tension and impacted -side compression. The fatigue test conditions are as follows: the loading form is a sine wave, the loading ratio is 0.1, and the frequency is 1.5 Hz. In the fatigue bending test, the maximum loading and bending stresses were measured when the specimen was fractured during the fatigue test.

The fracture bending stresses were measured on the assumption that the specimens were homogeneous isotropic materials (Malvern et al., 1989), because the stresses of CFRP laminates are linearly proportional to strain up to the point of rupture. The effects of dimension error can be eliminated by using a true measurement (i. e. at a width and thickness of a specimen).

The fracture bending stress equation is as follows:

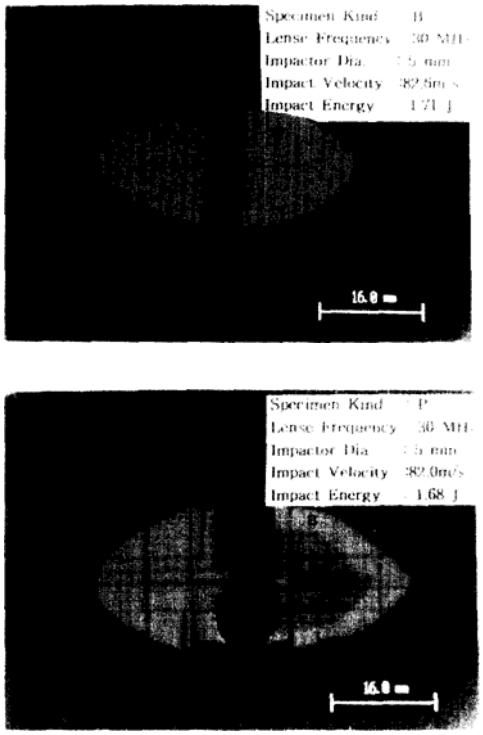

Fig. 4 Delamination shapes of specimens B, P.

$$I=\frac{bd^3}{12}$$

$$\sigma=\frac{(PL/4)(d/2)}{I}=\frac{3PL}{2bd^2} \quad (1)$$

where σ is the bending stress (GPa), P is the maximum loading at fracture (N), L is the length of span (m), b is the width of specimen (m), d is the thickness of specimen (m) and I is the moment of inertia (m4).

3. Discussion

3.1 Impact damages and damage growth observation

In the case of impact-induced CFRP laminates subjected to cycle loadings, initial impact damages in the interfaces are observed by using the SAM to investigate the failure mechanisms, and impact-damaged growth is observed every cycle until fractured.

Figure 4 shows the typical delamination shapes of specimens B and P and A and B indicate

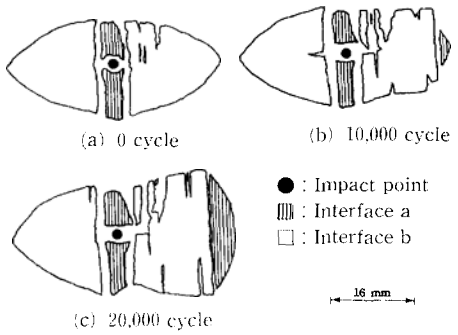

Fig. 5 Damage growth of specimen B during fatigue bending test when the impacted side is under tension (Impact energy : 1.68J).

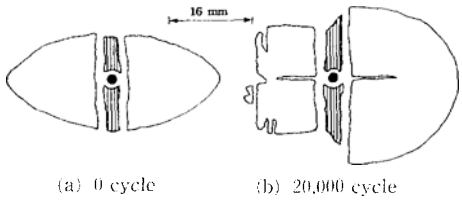

Fig. 6 Damage growth of specimen B during fatigue bending test when the impacted side is compressed (Impact energy : 1.71J).

interfaces A and B respectively. Figure 5 shows the damage growth direction in the case of impacted-side tension using the three-point fatigue bending test, and Fig. 5 (a), (b) and (c) indicate the delamination shapes after 0, 10,000 and 20,000 cycles respectively. Figure 6 shows the damage growth direction in the case of impacted-side compression, and Fig. 6 (a) and (b) indicate the delamination shapes after 0 and 20,000 cycles respectively. From Fig. 5 (b), (c), fracture is developed toward the impact point from the edge of interface B delamination after 10,000 cycles. The damaged-growth width increases from the edge after 20,000 cycles, and the specimen is fractured after 21,000 cycles. On the other hand, Fig. 6 shows that fracture is propagated from the transverse crack generated near the impact point in the case of impacted-side compression, and eventually fracture is generated along the transverse crack after 20,600 cycles.

Also, Fig. 7 shows the damage growth shapes of the impact-damaged specimen P in the case of

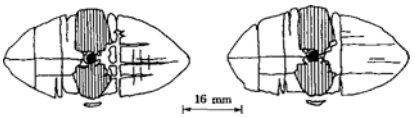

(a) 0 cycle (b) 2,000 cycle

● : Impact point ▥ : Interface a □ : Interface b

Fig. 7 Damage growth of specimen P during fatigue bending test when the impacted side is under tension (Impact energy : 1.71J).

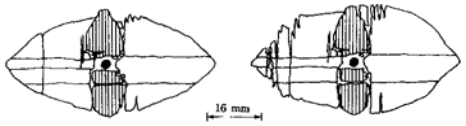

(a) 0 cycle (b) 5,000 cycle

● : Impact point ▥ : Interface a | | : Interface b

Fig. 8 Damage growth of specimen P during fatigue bending test when the Impacted side is compressed (Impact energy : 2.50J).

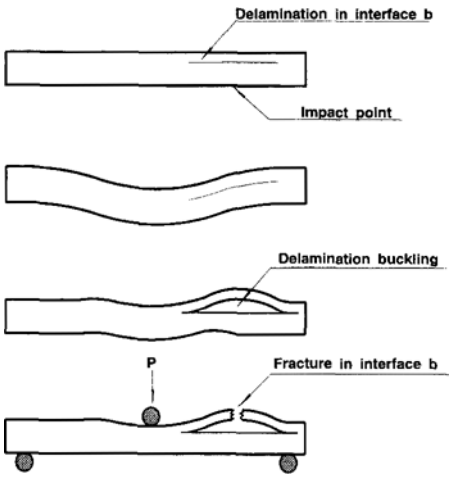

Fig. 9 Model of delamination buckling mode of specimen P.

impacted-side tension. Figure 8 shows the damage growth shapes of the impact-damaged specimen P (2.50J) in the case of impacted-side compression. From Fig. 7, almost no damage growth of specimen P appears in the case of impacted -side tension, but the specimen is fractured by local delamination buckling due to the delamination section of interface ***b*** subjected to compression as shown in Figs 9 and 8 shows the damage growth direction of specimen P in the case of

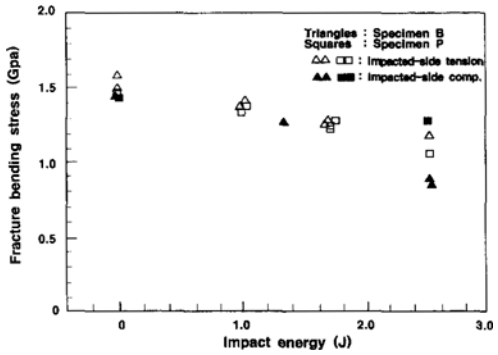

Fig. 10 Relation between impact energy and fracture bending stress of specimens B, P.

impacted-side compression, and fracture develops from the impact point at the transverse cracks as shown in Fig. 6.

However, the decreasing phenomena of fatigue bending strength in the case of laminates using PEEK matrix do not appear more often than using EPOXY matrix, and the damage growth of specimen P is generated later than that of specimen B.

3.2 Results of the static and fatigue three -point bending test

After observing the interface damage range of the specimens with impact damage by the SAM, the static three-point bending test was performed to consider the decreasing relation of residual bending strength.

Figure 10 shows the relation between impact energy and fracture bending stress of specimens B and P for each case of impacted-side tension and impacted-side compression. In the case of unimpacted specimens as shown in Fig. 10, the residual bending strength of specimen B is greater than that of specimen P, but less residual strength decreasing phenomena of impact-damaged specimen P is generated than that of impact-damaged specimen B in the case of impacted-side compression; therefore it has been found that the residual strength for the specimen B decreases suddenly. Also, in the case of impacted-side tension, the local buckling is generated at the interface **b** section of specimen P, and then the strength radically decreases. Because the delamination

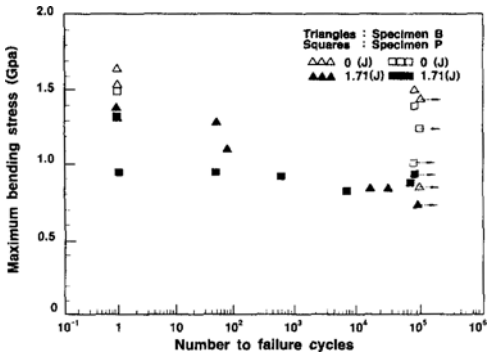

(a) Impacted side tension

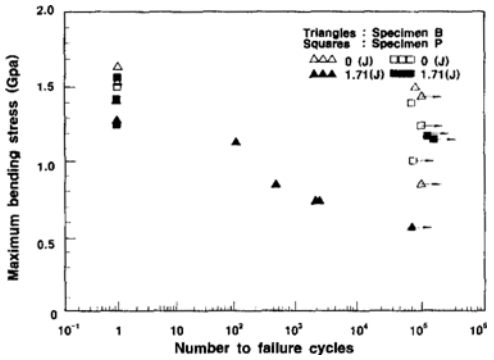

(b) Impacted side compression

Fig. 11 Residual fatigue bending strength of damaged specimens B, P.

length of interface **b** is longer as shown in Fig. 9, it is thought that the delamination section in interface **b** is compressed in the case of impacted -side tension. If the case of impacted-side tension is compared with the case of impacted-side compression, the strength in the case of impacted-side compression decreases much more than that in the case of impacted-side tension.

Figure 11 shows the fatigue test results of specimens B and P for each case of impacted-side tension and impacted-side compression. The Y -axis indicates the maximum bending stress, the X-axis indicates the number of cycles to failure and an arrow (→) indicates runway. From the results of the specimen B fatigue test, the fatigue strength in the impacted-side compression was slightly decreased from the impacted-side tension, as shown by the results of static bending test in Fig. 10. In the case of impacted-side compression, the fatigue strength of specimen B was radically decreased from that of specimen P, in which fatigue strength was constant to a certain extent. Also, in the case of unimpacted specimens B and P, the residual fatigue strengths are almost constant. The strength decreasing phenomena of specimen P are generated in the case of impacted-side tension for the impact-damaged specimen. Thus, it has been found that the delamination buckling generated at the impact side of interface b influences the fatigue bending strength as shown in the static test results.

4. Failure Mechanism

As described in Section 3-2, the damage growth is observed by the SAM to consider the decreasing relation of residual fatigue bending strength of specimen B for each case of impacted -side tension and impacted-side compression. Especially in the case of specimen B where the residual fatigue bending strength radically decreases, it is clear that the fractures grew at the transverse cracks, which occurred at an impact point by total delamination of interface **b** (90°/0°) under tension as shown in Fig. 10 for impacted -side compression. Also, it was found that the delamination width of interface **b** increased during the damage growth.

In the case of impacted-side tension as shown in Fig. 5, the transverse cracks are generated at the delamination edge of interface **b**. Contrary to impacted-side compression, it is known that the specimen fractures grew from the transverse cracks toward the impact point as the cycle loadings are repeated. From the damaged-growth shapes of Figs. 5 and 6, Figs. 12 and 13 show the fracture modes by conducting the fatigue bending test, using the specimens which were subjected to impact damages and show the delamination growth direction.

In the case of impacted-side compression shown in Fig. 10, the delaminations of interfaces **a** and **b** grew along the transverse cracks generated below the impact point, and the delamination possessing the greatest growth width was the

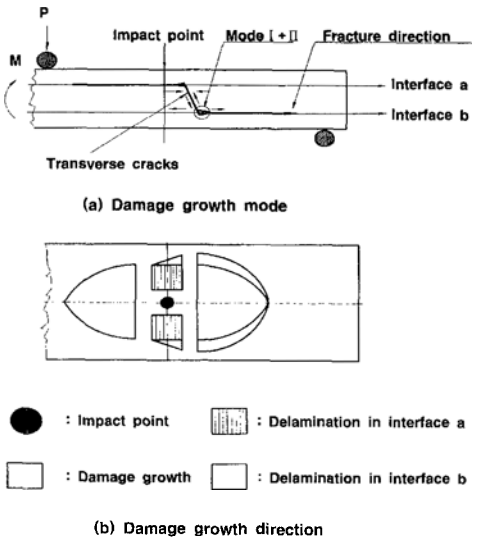

Fig. 12 Mechanism of damage growth during fatigue bending test when the impacted side is compressed.

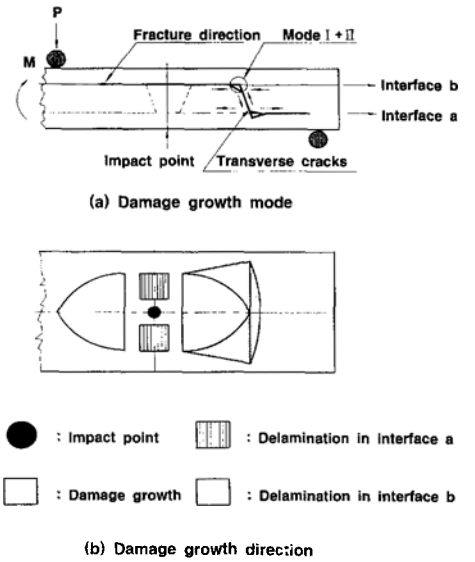

Fig. 13 Mechanism of damage growth during fatigue bending test when the impacted side is under tension.

delamination for interface **b** on the tension side.

To explain this phenomena, Fig. 12(a) shows in detail the fracture growth modes in consideration of shear stresses, tension and compression in the plane. When the transverse cracks extend in the tension direction in these modes, the opening displacement becomes greater, and when the cracks extend in the compression direction, closing phenomena occur.

Thus, because the opening displacements on the tension side (modes I + II) are higher than those on the compression side, delamination on the tension side can easily be extended. Therefore, when delamination develops in each ply, the interface modes can be assumed as shown in Fig. 12(a). The cause of transverse cracks occurring from impact loading reveals that the delaminations grew from the shearing strain generated during the three-point bending test. Fig. 12(b) shows the delamination and fracture surface growth direction. Also, in the case of impacted -side tension shown in Fig. 13(a), transverse cracks occur at the delamination edge of interface **b** on the compression side and it is known that the delamination of interface **b** grew toward the impact point. To explain these phenomena, Fig. 13(a) shows in detail the fracture growth modes in consideration of shear stresses, tension and compression in the plane. When the transverse cracks developed in the compression direction for the modes (modes I + II), the opening displacement in interface **b** becomes greater, in which case, delamination grows.

Therefore, delamination and growth direction can be assumed as shown in Fig. 13 (a), and delamination growth by shear strain causes each interface to fail. Fig. 13(b) shows the delamination and the growth direction. Thus, as shown in Figs. 12 and 13, the moment becomes greater because the radius of curvature at the fracture starting point was smaller in the case of impacted -side tension than in the case of impacted-side compression from the impact point. Therefore, it is thought that more fractures develop immediately under impacted-side compression than under impacted-side tension.

Also, the CFRP laminates subjected to impact damages are weaker under compression than under tension on the shock resistant.

5. Conclusions

After impacting on CFRP laminates, impact -induced growth was observed and the residual strength of the static and fatigue three-point bending test was evaluated. The phenomena of decreasing residual strength and its failure mechanisms were analyzed according to the matrices.

The conclusions are as follows:

(1) It has been found that the decreasing phenomena of residual fatigue bending strength in the case of impacted-side compression appear greater than in the case of impacted-side tension for the specimen B using EPOXY matrix.

(2) When the impacted side is compressed, the residual fatigue bending strength of the CF/PEEK specimen P is greater than that of the CF/EPOXY specimen B. On the other hand, when the impacted side is under tension, the residual fatigue bending strength of the CF/PEEK specimen P is smaller than that of CF/EPOXY specimen B since the delamination areas of the more highly damaged interface **b** are locally buckled and fractured in the case of impacted-side tension of the CF/PEEK laminates.

(3) In the case of impacted-side compression, fracture is propagated from the transverse crack generated near the impact point. On the other hand, fracture develop toward the impact point from the edge of interface **b** delamination in the case of impacted-side tension.

References

Bakis, C. E. and Stinchcomb, W. W. (Hahn H. H), 1989, "Response of Thick, Notched Laminates Subjected to Tension-Compression Cycle Loads", *Composite Materials : Fatigue and Fracture,* ASTM STP, 907, pp. 314~438.

Challenger, K. D., 1986, "The Damage Tolerance of Carbon Fiber Reinforced Composites", A workshop summary, *Composite Struct.,* pp. 295~318.

Ishai, O. and Shragi, A., 1990, "Effect of Impact Loading on Damage and Residual Compressive Strength of CFRP Laminated Beams," *Composite Struct.,* 14-4, pp. 319~337.

Ma, C. C. M., Huang, Y. H., and Chang, M. J., 1991, "Hygrothermal Effect on the PEEK/C. F. and PPS/C. F. Under Impact Loading(I)," *ANTEC,* pp. 2029~2096.

Malvern, L. E., Sun, C. T. and Liu, D., 1989, " Delamination Damage in Central Impacts at Subperformation Speeds on Laminated Kevlar/Epoxy Plates," *ASTM. STP.* 1012, pp. 387~405.

Rotem, A. and Nelson, H. G., 1990, "Residual Strength of Composite Laminate Subjected to Tensile-Compressive Fatigue Loading," *Journal of Composites Technology & Research,* Vol. 12, No. 2, pp. 76~84.

Smith, B. W. and Grove, R. A., 1987, "Determination of Crack Propagation Directions in Graphite/Epoxy Structures," *Composites and Metals,* ASTM. STP. 948, pp. 154~173.

Takeda T., 1985, "Impulsive Response and Fracture of Composites (I)," *Journal of the Japan Society for Composite Materials,* Vol. 11, No. 4, pp. 151~161.

Tanaka T., Kurokawa T., etc., 1989, "Damage and Residual Bending Strength of Graphite/Epoxy Composite Laminates Subjected to Normal Impact," *Journal of the Japan Society for Aeronautical & Space Sciences,* Vol. 37, No. 25, pp. 29~36.

Yang I. Y., Sim J. K. and Im K. H., 1996, "Impact Damages and Residual Bending Strength of CFRP Composite Laminates Subjected to Impact Loading," *KSME International Journal,* Vol. 10, No. 4, pp. 423~434